Theory of non-integer high-harmonic generation in a topological surface state

Maximilian Graml, Maximilian Nitsch,* Adrian Seith, Ferdinand Evers, and Jan Wilhelm†
Institute of Theoretical Physics, University of Regensburg, Universitätsstraße 31, D-93053 Regensburg, Germany
(Dated: May 6, 2022)

High harmonic generation is a versatile experimental technique for probing ultrafast electron dynamics. While in the past it has been employed typically in dielectrics and semiconductors, recently high harmonic generation was also observed from a topological surface [Schmid *et al.*, Nature **593**, 385 (2021)]. It has been found that harmonic orders in the intermediate range of 13 – 18 continuously shift when the carrier envelope phase (CEP) is varied. In this work, we adopt a minimal model of the topological surface state and calculate analytically the high-harmonic spectrum. We derive formulæ describing the parametric dependencies of CEP shifts in high harmonics; in particular, we have a transparent result for the shift of the (peak) frequency ω when changing the CEP φ: $d\omega/d\varphi = -2\bar{\mathfrak{f}}'\omega/\omega_0$, where ω_0 describes the fundamental driving frequency and $\bar{\mathfrak{f}}'$ characterizes the chirp of the driving laser pulse. We compare the analytical formula to full-fledged numerical simulations finding only 17 % average absolute deviation in $d\omega/d\varphi$. Our analytical result is fully consistent with experimental observations. It therefore provides the first understanding of the phenomenon of CEP shifts in solids based on analytically derived parametric dependencies.

I. INTRODUCTION

High harmonic generation (HHG) is a unique fingerprint of ultrafast electron dynamics in solids[1–16]: It is generated when atomically strong electric fields drive charge currents that in turn emit electromagnetic radiation. In solids, such currents are understood as interband transitions and (semiclassical) intraband currents. The emitted light supports frequencies much higher than those of the driving field, see also Fig. 1 as an illustration. Since high harmonics are sensing acceleration processes of the charge carriers, HHG can be used for monitoring dynamical processes. The information thus incorporated allows to reconstruct band structures[12,13]; it reflects dynamical Bloch oscillations[3,6,17] and Berry phase effects[16].

In the past, HHG has been analyzed to study charge carrier dynamics in dielectrics[2,6,10,11] and semiconductors[3–5]. Fresh applications to three-dimensional topological insulators and their gapless surface states have been published recently[9,18]. These surface states have been argued to be an ideal platform for lightwave electronics[9,19]. This is because the suppression of backscattering due to the spin-momentum locking makes it easier to facilitate quantum control for long times.[9,19,20]

A distinct feature of HHG in the topological surface state is the effect of the carrier-envelope phase (CEP)[21] on the high-harmonic spectrum[9]: Under tuning of the CEP, the observed harmonic orders 13 – 18 experience a continuous shift to arbitrary, non-integer multiples of the driving frequency[9]. As a first illustration for this shift, Fig. 1 displays the strong dependence of HHG on two values of the CEP for the case of a topological surface state. CEP shifts in HHG have been observed before in the emission spectrum from semiconductors[3] and dielectrics[10,11], but the observed peak frequencies are discontinuous functions of the CEP[3,10,11], in contrast to continuous peak shifts in HHG from a topological surface state[9].

In this work, we develop a minimal semiclassical model that explains the CEP shifts in analytical terms, that have been observed experimentally and computationally in high harmonics from a topological surface state[9]. The main result of our work is that under a tuning of the CEP by $d\varphi$, the frequency ω of high harmonics shifts by

$$d\omega = -2\,\frac{\omega}{\omega_0}\,\bar{\mathfrak{f}}'\,d\varphi\,; \tag{1}$$

here, ω_0 describes the fundamental frequency and $\bar{\mathfrak{f}}'$ characterizes the chirp of the driving laser pulse. Formula (1) has been derived for a the case of a Dirac-type band structure and ignoring interband transitions. We take this as the reason why (1) does not feature electronic structure parameters. We further show that the formula is in line with CEP shifts observed in Ref. 9 and with an additional, extended set of simulations. Thus, the assumptions underlying our minimal model are validated. Our work thus is yet another stepping stone towards an improved understanding of the fundamental mechanisms and parametric dependencies governing HHG.

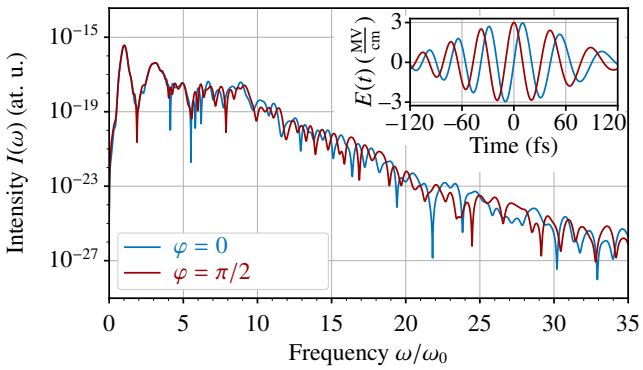

FIG. 1: High-harmonic emission spectrum $I(\omega)$ as function of the frequency ω computed from semiconductor Bloch equations (SBE)[14,22,23], Eq. (5). For the SBE simulation, we employ a two-band Hamiltonian[9] to model the topological surface state of Bi_2Te_3. As driving electric field $\mathbf{E}(t)$, we use Eq. (4) with $E_0 = 3\,\mathrm{MV/cm}$, $\omega_0 = 2\pi \cdot 25\,\mathrm{THz}$, $f_{\mathrm{chirp}} = -1.25\,\mathrm{THz}$, $\sigma = 90\,\mathrm{fs}$ as used in simulations in Ref. 9. We employ two different CEPs, $\varphi = 0$ (blue) and $\varphi = \pi/2$ (red). The driving electric field $E(t)$ is sketched in the inset.

II. MATHEMATICAL DEFINITION OF CEP SHIFTS

For deriving parametric dependencies of CEP shifts in high harmonics, we consider a CEP variation $\varphi \to \varphi + d\varphi$ in the driving electric field, see inset of Fig. 1 as an illustration. A formal definition of CEP shifts of high harmonics spectra $I(\omega)$ embarks on the observation that for a given $d\varphi$ a corresponding frequency shift $\omega \to \omega + d\omega$ can be found that leaves the emission unchanged, $dI = 0$.[24] We have

$$dI = (\partial I/\partial\omega)_\varphi \, d\omega + (\partial I/\partial\varphi)_\omega \, d\varphi \,, \tag{2}$$

and the condition $dI \stackrel{!}{=} 0$ translates into the definition of the frequency shift per CEP variation,

$$\frac{d\omega}{d\varphi} := -\frac{(\partial I/\partial\varphi)_\omega}{(\partial I/\partial\omega)_\varphi} \,. \tag{3}$$

In general, $d\omega/d\varphi$ is a function of ω and φ; $d\omega/d\varphi$ mathematically describes the tilt angle of the equi-intensity lines in the (ω, φ)-plane, which is observed in CEP-dependent high-harmonic spectra; see Fig. 2 for an illustration.

By integrating Eq. (3) one can find the equi-intensity line $\omega(\varphi)$ – for a fixed initial condition of integration, e.g. $\bar{\omega} := \omega(\varphi = 0)$; we denote this by $\omega_{\bar{\omega}}(\varphi)$. Intuitively speaking, $\omega_{\bar{\omega}}(\varphi)$ is the line in the map of $I(\omega, \varphi)$ that traces the equi-intensity line crossing the point $(\bar{\omega}, \varphi = 0)$.

III. CEP SHIFT FROM SBE SIMULATIONS

We start with numerical simulations of CEP shifts in high harmonics to illustrate the phenomenon and to motivate the minimal analytical model that we introduce later. For our theoretical analysis, we model the incoming laser pulse by the time-dependent electric field aligned in x-direction

$$\mathbf{E}(t) = \hat{\mathbf{x}} \, E_0 \sin\left(\omega_0 \left(1 + f_{\text{chirp}} t\right) t + \varphi\right) e^{-t^2/\sigma^2} \,, \tag{4}$$

with the parameters field strength E_0, CEP φ, and pulse duration σ. We employ the two-band model for the topological surface state of Bi_2Te_3 used in Ref. 9; it includes a Dirac cone at the Γ-point and the hexagonal warping in the band structure of the topological surface state[25]. Taking the pulse form and the model Hamiltonian as an input, we solve the semiconductor Bloch equations (SBE)[14,22,23] yielding the time-dependent density matrix $\rho(t)$. From this we obtain the physical current density $\mathbf{j}(t)$ and the emission spectrum $I(\omega)$,[23]

$$\mathbf{j}(t) := \frac{-e}{V} \operatorname{Tr}(\rho(t)\dot{\mathbf{r}}) \,, \qquad I(\omega) = \frac{\omega^2}{3c^2} \left|\mathbf{j}(\omega)\right|^2 \,, \tag{5}$$

where $-e/V$ is the electron charge density, $\dot{\mathbf{r}}$ the velocity operator, c the speed of light and $\mathbf{j}(\omega)$ the Fourier transform of $\mathbf{j}(t)$. We checked the convergence of observables with numerical parameters, see the Supporting Information (SI), Sec. S1.

The resulting high-harmonics spectrum $I(\omega)$ for pulse parameters adapted to experiment[9] is shown in Fig. 1, for a sine-like pulse ($\varphi = 0$) and a cosine-like pulse ($\varphi = \pi/2$): Both high-harmonics spectra are similar up to fifth harmonic order, $\nu = 5$,

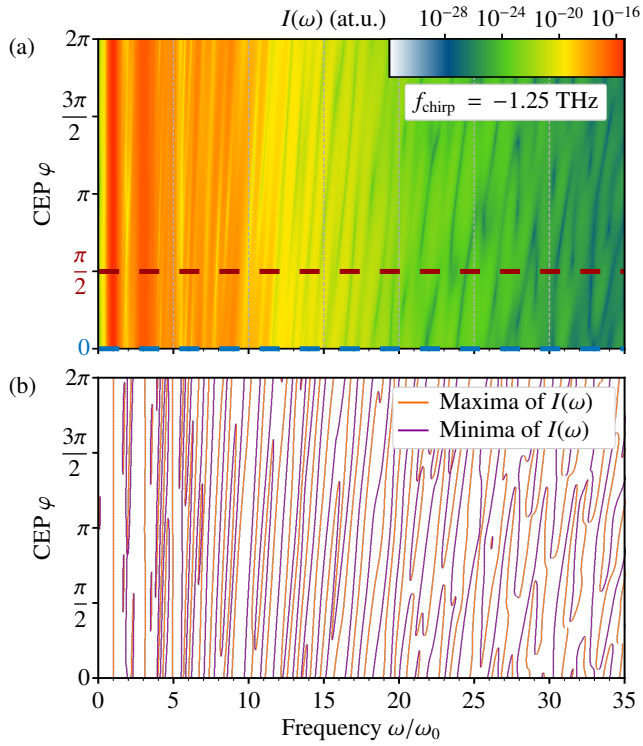

FIG. 2: (a) High-harmonics spectrum $I(\omega)$ computed from SBE, Eq. (5) for 384 discrete CEPs $\varphi \in [0, 2\pi]$ with $\mathbf{E}(t)$ and parameters as in Fig. 1. The heat map along the blue and red horizontal line (CEP $\varphi = 0$ and $\varphi = \pi/2$) represents the emission spectra from Fig. 1. (b) Local extrema of $I(\omega)$ from (a).

using a dimensionless frequency $\nu := \omega/\omega_0$. At higher frequencies, $14 \lesssim \nu \lesssim 20$, the two spectra differ in the sense that the maximum of one coincides with the minimum of the other. At even higher frequencies, $30 \lesssim \nu \lesssim 35$, maxima of the two spectra coincide and minima also coincide.

Similar to the experiment[9], we continuously vary the CEP from 0 to 2π, see Fig. 2 (a) and (b). We confirm the main experimental findings, albeit here observed in a much larger window, $5 \lesssim \nu \lesssim 35$, instead of $12 \lesssim \nu \lesssim 21$ in Ref. 9: The frequency shift grows at increasing harmonic order, which eventually leads to a pattern of tilted lines with tilt angle growing from left to right in Fig. 2 (b). Indications of an increase of the tilt-angle have been observed before in semiconductors and dielectrics, but the patterns there are less pronounced and systematical[10]. Presumably this is why a systematic theoretical understanding predicting parametric dependencies of CEP shifts has not been worked out.

IV. CEP SHIFTS FOR A SEMICLASSICAL MODEL – ANALYTICAL FORMULA

The systematic growth of the tilt angle with the high-harmonic order seen in Fig. 2 (b) suggests that there should be a simple analytical formula characterizing parametric de-

pendencies. In this section such a formula is derived within a minimal model.

We employ a semiclassical framework[26] neglecting anomalous velocity contributions[27]. Within this model, the electron velocity is given by

$$\mathbf{v}(t) = \left.\frac{\partial \epsilon}{\hbar\, \partial \mathbf{k}}\right|_{\mathbf{k}=\mathbf{k}(t)} . \tag{6}$$

$\mathbf{k}(t)$ is the excursion of the electron in reciprocal space. In semiclassics, $\mathbf{k}(t)$ fully characterizes the dynamics of the electron and is given by the Bloch acceleration theorem

$$\mathbf{k}(t) = \mathbf{k}_0 + \frac{1}{\hbar}\int_{-\infty}^{t} \mathbf{F}(t')\, dt' , \tag{7}$$

where $\mathbf{F}$ is the acting force, $\mathbf{F}(t) = -e\mathbf{E}(t)$, if only electric fields are to be accounted for. In our simplified approach we assume that the time dependence of $\mathbf{j}(t)$ is captured by $\mathbf{v}(t)$ taken at a characteristic wavenumber $\mathbf{k}_0$. For the purpose of calculating CEP shifts, prefactors - such as effective charge densities - can be ignored since they cancel for CEP shifts in Eq. (3).

We now analyze CEP shifts within the framework of model (6) and (7). Since it is assumed $\mathbf{j}(t) \propto \mathbf{v}(t)$, we have

$$I(\omega) \propto \omega^2 |\mathbf{v}(\omega)|^2 = |\partial_t \mathbf{v}(\omega)|^2 \tag{8}$$

from Eq. (5), where

$$\partial_t \mathbf{v}(\omega) := \int dt\; e^{-i\omega t}\, \partial_t \mathbf{v}(t) = \int dt\; e^{-i\omega t}\, \partial_t \left.\frac{\partial \epsilon}{\hbar\, \partial \mathbf{k}}\right|_{\mathbf{k}(t)} \tag{9}$$

is the Fourier transform of the time-dependent acceleration.

If the $\mathbf{k}$-derivative is analytic in the range of excursion of $\mathbf{k}(t)$, we may simplify

$$\begin{aligned}\partial_t v_i(\omega) &= \sum_j \int dt\; e^{-i\omega t} \left.\frac{\partial^2 \epsilon}{\hbar\, \partial k_i \partial k_j}\right|_{\mathbf{k}=\mathbf{k}(t)} \partial_t k_j(t) \\ &= -\frac{e}{\hbar}\sum_j \int dt\; e^{-i\omega t} \left.\frac{\partial^2 \epsilon}{\hbar\, \partial k_i \partial k_j}\right|_{\mathbf{k}=\mathbf{k}(t)} E_j(t).\end{aligned}$$

where we have $\partial_t k_j(t) = -eE_j(t)/\hbar$ in the absence of magnetic fields. It is a necessary condition for the generation of high harmonics that $\partial^2\epsilon/(\partial k_i \partial k_j)|_{\mathbf{k}=\mathbf{k}(t)}$ is time dependent. For the special case of parabolic dispersions with isotropic effective mass m we obtain

$$\partial_t \mathbf{v}(\omega) = -\frac{e}{m}\,\mathbf{E}(\omega) .$$

The conclusion is that parabolic dispersions do not exhibit HHG (within the validity of our minimal model).

As a minimal model for Dirac fermions we consider a linear dispersion

$$\epsilon(\mathbf{k}) = \hbar v_\mathrm{F} |\mathbf{k}| . \tag{10}$$

The velocity (6) for the linear dispersion is

$$\mathbf{v}(t) = \hat{\mathbf{x}}\, v_\mathrm{F}\, \mathrm{sgn}(k_x(t)) ; \tag{11}$$

the velocity is a constant, v_F, and it only changes its sign when $k_x(t)$ crosses zero. Hence, the acceleration $\partial_t \mathbf{v}(t)$ is a sequence of δ-functions in time with a corresponding Fourier transform

$$\partial_t \mathbf{v}(\omega) = 2v_\mathrm{F}\, \hat{\mathbf{x}} \sum_{m=1}^{N_z} (-1)^{m+1} \exp(i\omega t_m) . \tag{12}$$

The summation is over the zeros t_m of $k_x(t)$, which are readily obtained from (7); N_z denotes the number of these zeros (see SI, Sec. S2 for a formal derivation.) The zeros t_m will shift in the presence of a CEP, $t_m(\varphi)$. Since we require a 2π-periodicity in φ, we have $t_m(\pm 2\pi) = t_{m\pm p}(0)$, so after a full rotation a root m shifts into root $m \pm p$, p being integer.[28]

The emission intensity (8) corresponding to (12) reads

$$I(\omega) \propto |\partial_t \mathbf{v}(\omega)|^2 \propto \sum_{\ell,m}^{N_z} (-1)^{\ell+m} e^{i\omega t_{\ell m}(\varphi)} , \tag{13}$$

with $t_{\ell m}(\varphi) := t_\ell(\varphi) - t_m(\varphi)$. Then, Eq. (3) readily implies

$$\frac{d\omega}{d\varphi} = -\,\omega\,\frac{I_t'}{I_t} \tag{14}$$

where

$$I_t(\omega,\varphi) := \sum_{\ell,m}^{N_z} (-1)^{\ell+m} e^{i\omega t_{\ell m}(\varphi)} t_{\ell m}(\varphi) , \tag{15}$$

$$I_t'(\omega,\varphi) := \sum_{\ell,m}^{N_z} (-1)^{\ell+m} e^{i\omega t_{\ell m}(\varphi)} \partial_\varphi t_{\ell m}(\varphi) . \tag{16}$$

As an application, we consider the situation in which the CEP φ induces a homogeneous shift of all roots: $t_m(\varphi) = t_m(0) + \varphi/\omega_0$ and, in addition, an equidistant spacing $t_m(\pi) = t_{m+1}(0)$. Here implied is that $t_{\ell m}(\varphi)$ is independent of φ and therefore $I_t' = 0$. We conclude that a non-vanishing CEP shift requires that the zeros of $\mathbf{k}(t)$ are not equidistantly spaced.[29]

Non-equidistant roots of $\mathbf{k}(t)$ result from a time-dependent carrier frequency, which is defined as $(1 + \dot{\mathfrak{f}}(t))\omega_0$ ("chirp" $\dot{\mathfrak{f}}(t)$). In the SI, Sec. S3, we show that for small and slowly varying $\dot{\mathfrak{f}}(t)$, Eq. (14) simplifies to

$$\frac{d\omega}{d\varphi} = -2\,\frac{\omega}{\omega_0}\,\bar{\dot{\mathfrak{f}}}' , \tag{17}$$

where $\bar{\dot{\mathfrak{f}}}'$ is the average slope of $\dot{\mathfrak{f}}(t)$. Eq. (17) is our main result; it implies that under generic conditions the tilt angle $d\omega/d\varphi$ increases linearly in ω, and is independent of φ.

We now adress the shift of peak frequencies ω_peak in the high-harmonics spectrum, when changing the CEP from 0 to 2π, $\Delta\omega_\mathrm{peak} := \int_0^{2\pi} d\varphi\, (d\omega/d\varphi)$ along an equi-intensity line $\omega(\varphi)$. In the regime $|\bar{\dot{\mathfrak{f}}}'/\omega_0| \ll 1$ we focus on, $d\omega/d\varphi$ is only weakly dependent on the integration variable, because the relative change of $\omega(\varphi)$ along the equi-potential line is small: $\Delta\omega_\mathrm{peak} \ll \omega_\mathrm{peak}$; we thus approximate on the rhs of (17) $\omega(\varphi) \approx \omega(\varphi = 0) = \omega_\mathrm{peak}$, and arrive at the peak shift

$$\Delta\omega_\mathrm{peak} = -\,4\pi\,\frac{\omega_\mathrm{peak}}{\omega_0}\,\bar{\dot{\mathfrak{f}}}' . \tag{18}$$

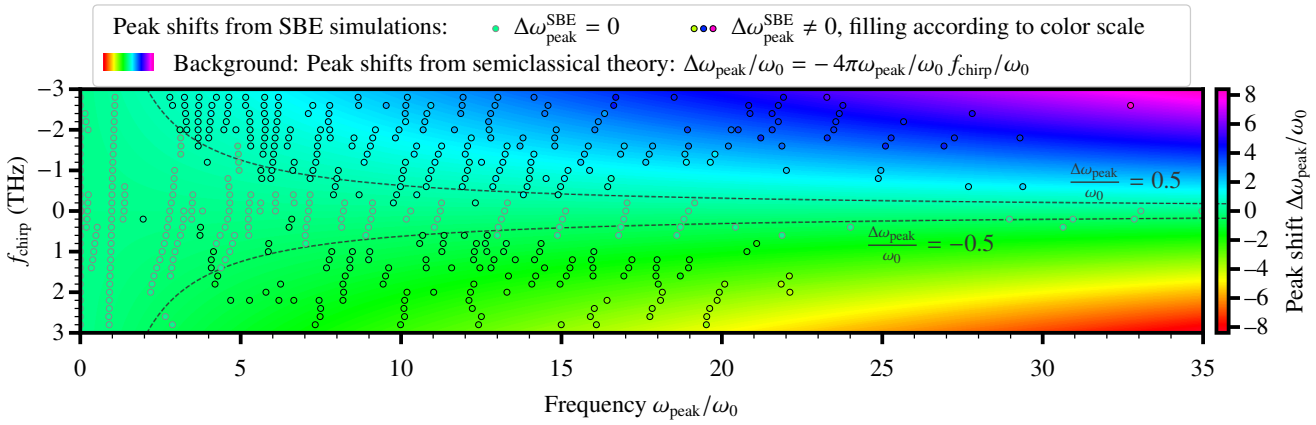

FIG. 3: Quantitative comparison of the peak shifts as obtained from the semiclassical model (18) (background, $\Delta\omega_{\rm peak}$) and from SBE simulations (color-filled circles, $\Delta\omega_{\rm peak}^{\rm SBE}$) in the parameter plane. $\Delta\omega_{\rm peak}^{\rm SBE}$ are obtained by tracing continuous maximum lines of the emission $I(\omega)$ as shown in Fig. 2 (b) from the initial point $(\omega_{\rm peak}^{\rm SBE}, \varphi=0)$ to the final point $(\omega_{\rm peak}^{\rm SBE}+\Delta\omega_{\rm peak}^{\rm SBE}, \varphi=2\pi)$. The dashed lines are guiding the eye; they indicate that best quantitative agreement is reached at peak-shifts exceeding 50% of ω_0. (For the SBE simulations, we considered 29 chirps with 384 CEPs each resulting in 11136 SBE runs.)

As an application of Eqs. (17) and (18), we consider an archetypical electric-field pulse (4), implying $\bar{\dot{\mathfrak{f}}}' = f_{\rm chirp}$, and small filling, i.e., $k_{\rm F}$ far away from all Brillouin zone boundaries, motivating a non-vanishing $|\mathbf{k}_0| \lesssim k_{\rm F}$. In this case the number of roots of $\mathbf{k}(t)$, N_z, is bounded: at infinite times the integral in (7) vanishes (since $\mathbf{E}(\omega=0)=0$) so that $\mathbf{k}(t)$ takes a non-vanishing limiting value.

Eq. (17) takes a simple form; while the frequency ω and the detuning per period $\bar{\dot{\mathfrak{f}}}'/\omega_0$ enter, other material or system parameters do not. The absence of $v_{\rm F}$ follows from the fact that the CEP is given as an intensity ratio, Eq. (3). Similarly, the envelope parameter σ of the driving electric field (4) (parameterized via N_z) cancels since our approximations imply $I_t' \propto I_t$.

The linear dependency of $d\omega$ on the chirp parameter $\bar{\dot{\mathfrak{f}}}'$ is rationalized as follows: By definition, the chirp accounts for the non-linear spacing of the roots of $\mathbf{k}(t)$. Therefore, in the absence of chirp, the CEP translates all roots by the same amount and therefore can be eliminated by a redefinition of the origin of time, $t \to t - d\varphi/\omega_0$. Thus, at $\bar{\dot{\mathfrak{f}}}'=0$ the current and the emission spectrum are both independent of φ resulting in the absence of CEP shifts, $d\omega = 0$. At non-vanishing chirp, corrections arise already at linear-order, $d\omega \propto \bar{\dot{\mathfrak{f}}}'$, reflecting the fact that the tilt $d\omega/d\varphi$ can take either sign.

Finally, the proportionality $d\omega \propto \omega/\omega_0$ can be understood by recalling that the electrons perform a number of ω/ω_0 cycles during a single fundamental period of $E(t)$. They thus can be expected to be more sensitive to a parametric change in $E(t)$, for example a change of $\bar{\dot{\mathfrak{f}}}'$, by a factor of ω/ω_0.

V. COMPARISON OF SEMICLASSICS TO SBE SIMULATIONS AND EXPERIMENTS

We proceed with a comparison of the semiclassical, analytical formulæ (17), (18) to SBE simulations and experiments[9].

In Fig. 2 we display SBE simulations of the CEP-dependent high-harmonic spectra. A straight-line character of the extremal lines – and correspondingly also the equi-intensity lines – is seen which is synonymous with a minor tilt-angle dependency on CEP φ; further the tilt angle $d\omega/d\varphi$ increases with ω. Both observations are fully consistent with our main result Eq. (17).

With respect to the sign of the tilt, we further observe in Fig. 2 that the extremal lines are tilted to the right (from south west to north east) which implies a positive tilt angle, $d\omega/d\varphi \geq 0$. The sign agrees with the semiclassical prediction (17), since we evaluate for the pulse (4) a negative $\bar{\dot{\mathfrak{f}}}'$ implying $d\omega/d\varphi \geq 0$ (for $\omega \geq 0$); specifically $\bar{\dot{\mathfrak{f}}}' = f_{\rm chirp} = -1.25$ THz.

For a quantitative comparison, we focus on peak shifts $\Delta\omega_{\rm peak}$. From the SBE simulations Fig. 2 (b), we extract peak shifts by tracing continuous maximum lines ("percolating lines") of the emission $I(\omega)$ connecting the points in the parameter plane $(\omega_{\rm peak}^{\rm SBE}, \varphi=0)$ and $(\omega_{\rm peak}^{\rm SBE}+\Delta\omega_{\rm peak}^{\rm SBE}, \varphi=2\pi)$. We obtain pairs of $(\Delta\omega_{\rm peak}^{\rm SBE}/\omega_{\rm peak}^{\rm SBE})$ as (1.0/10.2), (1.6/19.7), (2.2/24.7). Based on equation (18) we expect a ratio $\Delta\omega_{\rm peak}/\omega_{\rm peak} = -4\pi\bar{\dot{\mathfrak{f}}}'/\omega_0 = 0.1$, in good quantitative agreement with the extracted SBE data (simulation parameters: $\omega_0 = 2\pi\cdot 25$ THz and $\bar{\dot{\mathfrak{f}}}' = f_{\rm chirp} = -1.25$ THz). We proceed and calculate the peak shifts $\Delta\omega_{\rm peak}$ for a collection of chirps to test the limits of (18) in the plane spanned by $\omega_{\rm peak}$ and $f_{\rm chirp}$. Fig. 3 shows the (color-coded) semiclassical result (18). The color-filled circles superimposed to the colored, semiclassical "background" indicate the corresponding SBE results, $\Delta\omega_{\rm peak}^{\rm SBE}$; the circle-colors follow the same scale abopted also for the semiclassical data.

In Fig. 3, we observe that SBE peak shifts (circles) are in good overall quantitative agreement with the semiclassical prediction (background): the color of the circular discs matches the background. (Averaging over the entire plane, we compute a mean absolute deviation of only 0.21 ω_0.)

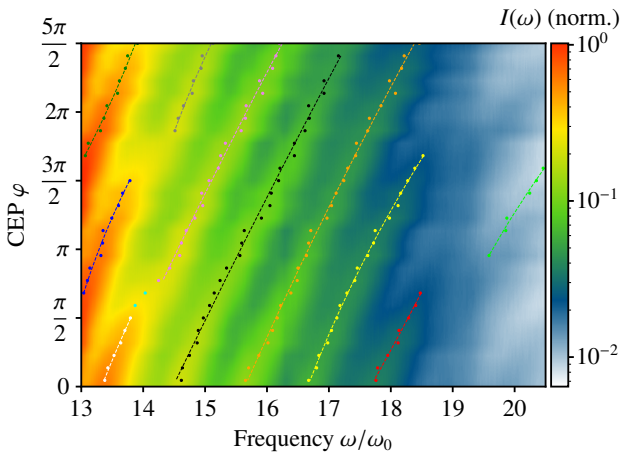

FIG. 4: CEP-dependency of the high-harmonics spectrum of Bi_2Te_3; experimental data taken from Ref. 9. We report local maxima as colored dots. We form sets of local maxima, as indicated by the various colors. For each set, we perform a quadratic fit $\omega(\varphi) = \omega_0[\alpha + \beta(\varphi - \bar{\varphi}) + \gamma(\varphi - \bar{\varphi})^2]$ (dotted lines, $\bar{\varphi}$ is fixed as the average CEP of a line segment, fit parameters α, β, γ are reported in Table I and SI-Table S1).

TABLE I: Fit parameter β (tilt angle) of fits reported in Fig. 4, as function of the average frequency $\bar{\omega}$ of the line segment.

$\bar{\omega}/\omega_0$	13.4	13.5	13.6	14.8	15.3	15.8	17.0	17.5	18.1	20.1
$2\pi\beta$	1.81	2.00	1.89	1.86	2.23	2.25	2.19	2.24	2.39	2.84

At weak chirp and small peak frequencies (low harmonics), the SBE-simulations exhibit many vertical maximum-intensity lines; the corresponding peak shifts vanish. These vanishing peak shifts appear in a region in the phase diagram Fig. 3, which reveals itself as the area that supports light gray circles. The region has a characteristic boundary corresponding to $|\Delta\omega_{\text{peak}}| \leq 0.5\,\omega_0$; it is indicated by the dashed lines in Fig. 3. Within this region, the relative discrepancy to the semiclassical model is somewhat enhanced. Outside this region, we find the mean relative absolute deviation in the peak shift to be only 17 % between SBE simulations and the semiclassical formula (18).

We compare our findings (14) and (17) to the experimental high-harmonics spectra emitted from a topological surface state[9]. The experimental data, Fig. 4, indeed displays the characteristic stripe pattern that our theoretical analysis predicts. Beyond this, there is also a qualitative agreement in details; e.g., the increase of the tilt angle with growing harmonic order predicted in (17) is also seen in Fig. 4.

For a quantitative analysis, we fit parabolas to discrete local maxima, see Fig. 4. We find that the linear order is dominating the fit, in line with our analytical result (17). From our quantitative analysis, we also find that tilt angle tends to increase with the frequency, see Table I. From 14th to 19th order we observe a "locking effect", i.e., the average tilt angle between 15th and 18th harmonic order is identical within at most 3 % (Table I). This locking effect is directly related to an equidistant placement of the maxima. Locking effects and equidistant placement of maxima are also seen in SBE simulations, Fig. 2.

The linear tilts of the fits together with the analytical result (17) give an estimate for the pulse-shape parameter, $2\pi\bar{\mathfrak{f}}'/\omega_0 = -0.067 \pm 0.001$. The experimental pulse shape has actually been reported in Ref. 9, so that $\bar{\mathfrak{f}}'$ can be directly calculated for the given pulse as $-2\pi\bar{\mathfrak{f}}'/\omega_0 \approx 0.037$, see SI, Sec. S4, which is only ~ 55 % of the fitted value. We assign this quantitative discrepancy to the fact that the experimental pulse shape does not match the condition for the applicability of the semiclassical formula (17), which is that the curvature $\mathfrak{f}''(t)$ is negligible, see SI, Sec. S4 for a detailed analysis.

The validity of the formulae (17)/(18) even outside the strict limits for its derivation deserves a special attention. Indeed, the main requirement for the applicability of the arguments that constitute our semiclassical theory is that the charge carrier acceleration changes abruptly on a time scale that is very short compared to the intrinsic time scales of the laser pulse. Then, the expressions for the dynamical forces, Eq. (12), and the high-harmonics emission, Eq. (13), are faithful representations. We expect that this basic requirement is fulfilled whenever there are sharp features or transitions, e.g., in the band structure or in the laser-pulse itself. Correspondingly, the semiclassical ansatz should be reliable also for more general situations than considered in our explicit analytical calculations, such as the presence of multiple bands, interactions and even dissipation. This robustness ensures the general applicability of our semiclassical arguments to full-fledged SBE simulations and, in particular, also to real experiments[9].

VI. CONCLUSION

We propose a semiclassical theory for the carrier envelope phase (CEP) dependency of high-harmonic generation under illumination of a material with strong laser pulses. The central result is a semiclassical theory that provides, in particular, an analytical formula describing the shifts of high-harmonic peaks under the change of the CEP. This formula explains, e.g., why peak positions can occur at non-integer harmonic orders. Further, it predicts that the shift velocity is proportional to the peak frequency and the chirp of the driving laser pulse. The comparison with a full-fledge simulation based on the semiconductor-Bloch formalism establishes the quantitative accuracy of the semiclassical result in a large parameter regime. Also the comparison to the experiment[9] works out in quantitative terms. We believe that our theory provides the first understanding of the phenomenon of CEP shifts in solids based on analytically derived parametric dependencies. Finally, we emphasize that our theory is broadly applicable since the main condition being the existence of sharp features in the band structure of the material hosting the charge carriers. Our work is thus another stepping stone towards understanding the microscopic mechanisms underlying high-harmonic generation in solids.

CODE AVAILABILITY

For all SBE simulations, we have used our program package CUED[23], that is freely available, https://github.com/ccmt-regensburg/CUED.

AUTHOR CONTRIBUTIONS

M.G. carried out SBE simulations and analyzed the numerical data. M.N, M.G., F.E., and J.W. developed the analytical model. A.S. developed the SBE simulation code. F.E. and J.W. conceived the study, supervised the project and wrote the paper with contributions from all authors. All authors contributed to discussing the results.

ACKNOWLEDGMENTS

We thank P. Grössing, C. Schmid, and L. Weigl for helpful discussions. We acknowledge support from the German Research Foundation (DFG) through the Collaborative Research Center, SFB 1277 (project A03) and through the State Major Instrumentation Programme, No. 464531296. The authors gratefully acknowledge the Gauss Centre for Supercomputing e.V. (www.gauss-centre.eu) for funding this project by providing computing time on the GCS Supercomputer SuperMUC-NG at Leibniz Supercomputing Centre (www.lrz.de) via project pn72pa.

* Present adress: NanoLund and Solid State Physics, Lund University, Box 118, 22100 Lund, Sweden
† jan.wilhelm@physik.uni-regensburg.de

[1] A. H. Chin, O. G. Calderón, and J. Kono, Phys. Rev. Lett. **86**, 3292 (2001).
[2] S. Ghimire, A. D. DiChiara, E. Sistrunk, P. Agostini, L. F. DiMauro, and D. A. Reis, Nat. Phys. **7**, 138 (2011).
[3] O. Schubert, M. Hohenleutner, F. Langer, B. Urbanek, C. Lange, U. Huttner, D. Golde, T. Meier, M. Kira, S. W. Koch, and R. Huber, Nat. Photonics **8**, 119 (2014).
[4] M. Hohenleutner, F. Langer, O. Schubert, M. Knorr, U. Huttner, S. W. Koch, M. Kira, and R. Huber, Nature **523**, 572 (2015).
[5] G. Vampa, T. Hammond, N. Thiré, B. Schmidt, F. Légaré, C. McDonald, T. Brabec, and P. Corkum, Nature **522**, 462 (2015).
[6] T. T. Luu, M. Garg, S. Y. Kruchinin, A. Moulet, M. T. Hassan, and E. Goulielmakis, Nature **521**, 498 (2015).
[7] M. Garg, M. Zhan, T. T. Luu, H. Lakhotia, T. Klostermann, A. Guggenmos, and E. Goulielmakis, Nature **538**, 359 (2016).
[8] N. Yoshikawa, T. Tamaya, and K. Tanaka, Science **356**, 736 (2017); H. A. Hafez, S. Kovalev, J.-C. Deinert, Z. Mics, B. Green, N. Awari, M. Chen, S. Germanskiy, U. Lehnert, J. Teichert, Z. Wang, K.-J. Tielrooij, Z. Liu, Z. Chen, A. Narita, K. Müllen, M. Bonn, M. Gensch, and D. Turchinovich, Nature **561**, 507 (2018).
[9] C. P. Schmid, L. Weigl, P. Grössing, V. Junk, C. Gorini, S. Schlauderer, S. Ito, M. Meierhofer, N. Hofmann, D. Afanasiev, J. Crewse, K. A. Kokh, O. E. Tereshchenko, J. Güdde, F. Evers, J. Wilhelm, K. Richter, U. Höfer, and R. Huber, Nature **593**, 385 (2021).
[10] Y. S. You, M. Wu, Y. Yin, A. Chew, X. Ren, S. Gholam-Mirzaei, D. A. Browne, M. Chini, Z. Chang, K. J. Schafer, M. B. Gaarde, and S. Ghimire, Opt. Lett. **42**, 1816 (2017).
[11] M. Sivis, M. Taucer, G. Vampa, K. Johnston, A. Staudte, A. Y. Naumov, D. M. Villeneuve, C. Ropers, and P. B. Corkum, Science **357**, 303 (2017); M. Garg, H. Y. Kim, and E. Goulielmakis, Nat. Photonics **12**, 291 (2018).
[12] G. Vampa, T. J. Hammond, N. Thiré, B. E. Schmidt, F. Légaré, C. R. McDonald, T. Brabec, D. D. Klug, and P. B. Corkum, Phys. Rev. Lett. **115**, 193603 (2015).
[13] N. Tancogne-Dejean, O. D. Mücke, F. X. Kärtner, and A. Rubio, Nat. Commun. **8**, 745 (2017).
[14] L. Yue and M. B. Gaarde, J. Opt. Soc. Am. B **39**, 535 (2022).
[15] J. Park, A. Subramani, S. Kim, and M. F. Ciappina, Adv. Phys.: X **7**, 2003244 (2022).
[16] T. T. Luu and H. J. Wörner, Nat. Commun. **9**, 916 (2018); H. Liu, Y. Li, Y. S. You, S. Ghimire, T. F. Heinz, and D. A. Reis, Nat. Phys. **13**, 262 (2017); R. Silva, Á. Jiménez-Galán, B. Amorim, O. Smirnova, and M. Ivanov, Nat. Photonics **13**, 849 (2019); D. Bauer and K. K. Hansen, Phys. Rev. Lett. **120**, 177401 (2018); H. Drüeke and D. Bauer, Phys. Rev. A **99**, 053402 (2019); C. Jürß and D. Bauer, Phys. Rev. B **99**, 195428 (2019); Phys. Rev. A **102**, 043105 (2020); D. Moos, C. Jürß, and D. Bauer, Phys. Rev. A **102**, 053112 (2020); A. Chacón, D. Kim, W. Zhu, S. P. Kelly, A. Dauphin, E. Pisanty, A. S. Maxwell, A. Picón, M. F. Ciappina, D. E. Kim, C. Ticknor, A. Saxena, and M. Lewenstein, Phys. Rev. B **102**, 134115 (2020); D. Baykusheva, A. Chacón, D. Kim, D. E. Kim, D. A. Reis, and S. Ghimire, Phys. Rev. A **103**, 023101 (2021); D. Baykusheva, A. Chacón, J. Lu, T. P. Bailey, J. A. Sobota, H. Soifer, P. S. Kirchmann, C. Rotundu, C. Uher, T. F. Heinz, D. A. Reis, and S. Ghimire, Nano Lett. **21**, 8970 (2021); Z. Lou, Y. Zheng, C. Liu, Z. Zeng, R. Li, and Z. Xu, Opt. Express **29**, 37809 (2021); A. Bharti, M. S. Mrudul, and G. Dixit, Phys. Rev. B **105**, 155140 (2022).
[17] M. Borsch, C. P. Schmid, L. Weigl, S. Schlauderer, N. Hofmann, C. Lange, J. T. Steiner, S. W. Koch, R. Huber, and M. Kira, Science **370**, 1204 (2020).
[18] Y. Bai, F. Fei, S. Wang, N. Li, X. Li, F. Song, R. Li, Z. Xu, and P. Liu, Nat. Phys. **17**, 311 (2021).
[19] J. Reimann, S. Schlauderer, C. P. Schmid, F. Langer, S. Baierl, K. A. Kokh, O. E. Tereshchenko, A. Kimura, C. Lange, J. Güdde, U. Höfer, and R. Huber, Nature **562**, 396 (2018).
[20] F. Giorgianni, E. Chiadroni, A. Rovere, M. Cestelli-Guidi, A. Perucchi, M. Bellaveglia, M. Castellano, D. Di Giovenale, G. Di Pirro, M. Ferrario, R. Pompili, C. Vaccarezza, F. Villa, A. Cianchi, A. Mostacci, M. Petrarca, M. Brahlek, N. Koirala, S. Oh, and S. Lupi, Nat. Commun. **7**, 11421 (2016).
[21] D. J. Jones, S. A. Diddams, J. K. Ranka, A. Stentz, R. S. Windeler, J. L. Hall, and S. T. Cundiff, Science **288**, 635 (2000); G. G. Paulus, F. Grasbon, H. Walther, P. Villoresi, M. Nisoli, S. Stagira, E. Priori, and S. De Silvestri, Nature **414**, 182 (2001); S. T. Cundiff and J. Ye, Rev. Mod. Phys. **75**, 325 (2003); A. Baltuška, T. Udem, M. Uiberacker, M. Hentschel, E. Goulielmakis, C. Gohle, R. Holzwarth, V. S. Yakovlev, A. Scrinzi, T. W. Hänsch, and F. Krausz, Nature **421**, 611 (2003).

[22] S. Schmitt-Rink, D. S. Chemla, and H. Haug, Phys. Rev. B **37**, 941 (1988); M. Lindberg and S. W. Koch, Phys. Rev. B **38**, 3342 (1988); C. Aversa and J. E. Sipe, Phys. Rev. B **52**, 14636 (1995); W. Schäfer and M. Wegener, *Semiconductor Optics and Transport Phenomena* (Springer, Heidelberg, 2002); H. Haug and A.-P. Jauho, *Quantum Kinetics in Transport and Optics of Semiconductors* (Springer, Heidelberg, 2008); H. Haug and S. W. Koch, *Quantum theory of the optical and electronic properties of semiconductors* (World Scientific Publishing Co., New York, 2009); M. Kira and S. W. Koch, *Semiconductor Quantum Optics* (Cambridge University Press, New York, 2011); P. Földi, Phys. Rev. B **96**, 035112 (2017); R. E. F. Silva, F. Martín, and M. Ivanov, Phys. Rev. B **100**, 195201 (2019); J. Li, X. Zhang, S. Fu, Y. Feng, B. Hu, and H. Du, Phys. Rev. A **100**, 043404 (2019); L. Yue and M. B. Gaarde, Phys. Rev. A **101**, 053411 (2020); L. H. Thong, C. Ngo, H. T. Duc, X. Song, and T. Meier, Phys. Rev. B **103**, 085201 (2021).

[23] J. Wilhelm, P. Grössing, A. Seith, J. Crewse, M. Nitsch, L. Weigl, C. Schmid, and F. Evers, Phys. Rev. B **103**, 125419 (2021).

[24] Other kinds of CEP shifts that also give useful characterizations of the $I(\omega,\varphi)$ map can be conceived, too. For example, rather than tracing lines with $dI=0$, one can trace maxima or minima, so requiring $d(\partial I/\partial\omega)_\varphi = 0$, see Fig. 2 (b) as an example. In analogy to Eq. (2), we then consider

$$d(\partial I/\partial\omega) = (\partial^2 I/\partial\omega^2)\,d\omega + (\partial^2 I/(\partial\omega\partial\varphi))\,d\varphi$$

which, together with the defining requirement $d(\partial I/\partial\omega)_\varphi = 0$, leads to an alternative set of lines $\omega(\varphi)$ in the ω-φ plane with tilt angle

$$\frac{d\omega}{d\varphi} \coloneqq -\frac{\partial^2 I/(\partial\omega\partial\varphi)}{\partial^2 I/\partial\omega^2}\,.$$

This definition and definition (3) are equivalent in case maxima and minima lines are also equi-intensity lines.

[25] C.-X. Liu, X.-L. Qi, H.-J. Zhang, X. Dai, Z. Fang, and S.-C. Zhang, Phys. Rev. B **82**, 045122 (2010).

[26] N. Ashcroft and N. Mermin, *Solid State Physics* (Saunders College, Philadelphia, 1976).

[27] D. Xiao, M.-C. Chang, and Q. Niu, Rev. Mod. Phys. **82**, 1959 (2010).

[28] Note that due to the special nature of the Dirac-dispersion, the acceleration $\partial_t \mathbf{v}$ does not scale with the applied force $-e\mathbf{E}$. The electric field enters only indirectly in the sense that for non-vanishing $\mathbf{k}_0$ a minimum field-strength is required to produce zeros in $\mathbf{k}(t)$.

[29] This conclusion has already been drawn in Refs. 10 and 30.

[30] M. V. Frolov, N. L. Manakov, A. A. Silaev, N. V. Vvedenskii, and A. F. Starace, Phys. Rev. A **83**, 021405 (2011); M. V. Frolov, N. L. Manakov, A. M. Popov, O. V. Tikhonova, E. A. Volkova, A. A. Silaev, N. V. Vvedenskii, and A. F. Starace, Phys. Rev. A **85**, 033416 (2012); A. Y. Naumov, D. M. Villeneuve, and H. Niikura, Phys. Rev. A **91**, 063421 (2015); G. Sansone, Phys. Rev. A **79**, 053410 (2009).

[31] I. Floss, C. Lemell, G. Wachter, V. Smejkal, S. A. Sato, X.-M. Tong, K. Yabana, and J. Burgdörfer, Phys. Rev. A (R) **97**, 011401 (2018).

[32] SciPy 1.0 Contributors, Nat. Methods **17**, 261 (2020).

[33] I. Al-Naib, J. E. Sipe, and M. M. Dignam, Phys. Rev. B **90**, 245423 (2014).

[34] H. J. Monkhorst and J. D. Pack, Phys. Rev. B **13**, 5188 (1976).

Supplementary material for

Theory of non-integer high-harmonic generation in a topological surface state

S1. COMPUTATIONAL DETAILS AND CONVERGENCE TESTS

As electric field, we use Eq. (4) throughout where the parameters $E_0 = 3\,\mathrm{MV/cm}$, $\omega_0 = 2\pi \cdot 25\,\mathrm{THz}$ and $\sigma = 90\,\mathrm{fs}$ were fixed for all calculations. We align the electric field along the Γ-M direction which we label as x-direction in Eq. (4). We have used the two-band Dirac-like model Hamiltonian for the topological surface states of Bi_2Te_3 from Ref. 9 together with a hexagonal Brillouin zone with a size that stems from a real space lattice constant $a = 4.396\,\text{Å}$. As in Ref. 9, we start from an equilibrium band occupation that is given by a Fermi-Dirac distribution with a Fermi level of 0.176 eV above the conduction band minimum and with a temperature of 30 meV. We compute the time-dependent density matrix $\rho(t)$ from SBE in the velocity gauge with a dephasing time $T_2 = 10\,\mathrm{fs}$ which is an accepted simulation value[31]. For the time evolution in the SBE formalism, we employ an adaptive algorithm[32] with a maximum time step of 0.1 fs and with a time window of $[-500\,\mathrm{fs}, 500\,\mathrm{fs}]$. These settings lead to intensity spectra that are converged with respect to time discretization. The Fourier transform to frequency domain includes a Gaussian window function with full width at half maximum of $2\sqrt{\ln 2} \cdot 90\,\mathrm{fs}$. In the SBE, dipoles are used which are diverging for the Dirac-like two-band Hamiltonian at the Γ-point[23,33]. Thus, we carefully checked the convergence of the k-point mesh, see Fig. S1. We observe excellent agreement between the 900×90 and 1800×180 k-mesh. We conclude that the 900×90 mesh is sufficient to reach convergence in the k-point mesh size and therefore, we have used a 900×90 mesh for all SBE calculations. In all figures, we have varied the CEP from 0 to 2π, where we have used $N_{\mathrm{CEP}} = 384$ discrete CEPs in the $[0, 2\pi]$ window thoughout.

S2. FOURIER TRANSFORM OF THE TIME-DEPENDENT CURRENT

The time derivative of the current (11) is

$$\partial_t \mathbf{v}(t) = -2\,\hat{\mathbf{x}}\,\frac{e v_{\mathrm{F}}}{\hbar}\,E(t)\,\delta(k_x(t))\,, \tag{S1}$$

where δ denotes the Dirac delta function. Then,

$$\delta(k_x(t)) = \sum_m \frac{\delta(t - t_m(\varphi))}{\left|\partial_t k_x(t)|_{t_m(\varphi)}\right|} = \sum_m \frac{\delta(t - t_m(\varphi))}{e\,|E(t_m(\varphi))|\,/\hbar}\,. \tag{S2}$$

Combining Eqs. (S1) and (S2), we arrive at Eq. (12),

$$\mathbf{v}(\omega) = \frac{1}{i\omega}\,\partial_t \mathbf{v}(\omega) = \frac{2 v_{\mathrm{F}}}{i\omega}\,\hat{\mathbf{x}} \sum_m (-1)^{m+1} \exp[i\omega t_m(\varphi)]\,. \tag{S3}$$

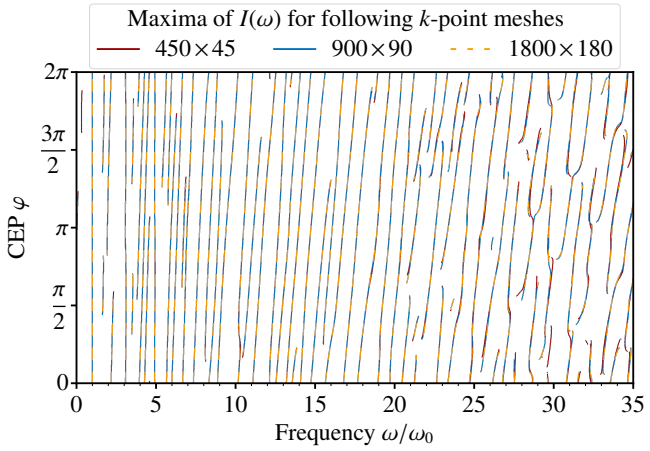

FIG. S1: Maxima of $I(\omega)$ computed with parameters as in Fig. 2 c for three different Monkhorst-Pack k-point meshes[34] $N_1 \times N_2$ (450×45, 900×90, 1800×180), where N_1 is the number of k-points in Γ-M direction and N_2 is the number of k-points orthogonal to the Γ-M direction.

The linear dispersion (10) of the model band structure is justified by the Dirac character of the surface conduction band of Bi_2Te_3 close to the Γ-point.[25] For the other commonly adopt model band structure, a parabolic dispersion $\epsilon(\mathbf{k}) = \hbar^2|\mathbf{k}|^2/(2m)$, no high-harmonic emission is observed under driving by an electric field from Eq. (4). This is due to the velocity $\mathbf{v}(t) = \hbar\mathbf{k}(t)/m$ [Eq. (6)] oscillating solely with the fundamental frequency ω_0.

We also do not consider excitonic effects and other electron-electron interaction during the non-equilibrium dynamics as they are believed to have negligible contributions[9]. Also, we omit bulk bands which have been shown to not contribute to the high-harmonic emission for the pulse shape we consider in this work[9].

S3. GENERAL DISCUSSION OF CEP-SHIFTS AT WEAK CHIRP

We give more details on the discussion of the spacing of roots in Sec. IV. The starting point is a homogeneous spacing, $t_m^{(0)}(\varphi) = (m\pi + \varphi)/\omega_0$ of the zeros of (7), $\mathbf{k}(t_m^{(0)}(\varphi)) = 0$, where ω_0 is the fundamental frequency. We achieve a non-uniform spacing by implementing a small rescaling of the time, $\mathbf{k}(t) \to \mathbf{k}(t(1 + \mathfrak{f}(t))$, such that we have for the zeros $t_m(\varphi)$ with non-uniform spacing

$$t_m^{(0)}(\varphi) = \left[1 + \mathfrak{f}(t_m(\varphi))\right] t_m(\varphi)\,. \tag{S4}$$

The chirp introduced in Sec. IV corresponds to a linear dependency $\mathfrak{f}(t) = -f_{\mathrm{chirp}}$. We consider more general situations subject to the condition that $\mathfrak{f}(t)$ is slowly varying from one zero to the next. Solving (S4) for t_m we have

$$\begin{aligned} t_m(\varphi) &= t_m^{(0)}(\varphi) - \mathfrak{f}(t_m^{(0)}(\varphi))\, t_m^{(0)}(\varphi) + O(\mathfrak{f}^2) \\ &\approx t_m^{(0)}(\varphi)\left[1 - \mathfrak{f}(t_m^{(0)}(\varphi))\right] \end{aligned} \tag{S5}$$

where gradient terms have been neglected. Further, after defining the equal spacing ($t_{\ell m}^{(0)} := t_\ell^{(0)}(\varphi) - t_m^{(0)}(\varphi) = \pi(\ell - m)/\omega_0 = t_{\ell-m}^{(0)}(\varphi{=}0)$), we define the non-uniform spacing $t_{\ell m}(\varphi) := t_\ell(\varphi) - t_m(\varphi)$

$$\begin{aligned} t_{\ell m}(\varphi) &\approx t_{\ell m}^{(0)} - \left[t_\ell^{(0)}(\varphi)\,\mathfrak{f}(t_\ell^{(0)}(\varphi)) - t_m^{(0)}(\varphi)\,\mathfrak{f}(t_m^{(0)}(\varphi))\right] \\ &\approx t_{\ell m}^{(0)}\left[1 - \mathfrak{f}(T_{\ell m}^{(0)}(\varphi)) - T_{\ell m}^{(0)}(\varphi)\,\mathfrak{f}'(T_{\ell m}^{(0)}(\varphi))\right] \end{aligned} \tag{S6}$$

where $T_{\ell m}^{(0)}(\varphi) := (t_\ell^{(0)}(\varphi) + t_m^{(0)}(\varphi))/2 = t_{(\ell+m)/2}^{(0)}(\varphi)$ and terms involving second derivatives have been dropped. Similarly, we have

$$\partial_\varphi t_{\ell m} = -2t_{\ell m}^{(0)}\,\mathfrak{f}'(T_{\ell m}^{(0)})/\omega_0 \tag{S7}$$

and Eqs. (15) and (16) are therefore to leading order in $\mathfrak{f}$

$$I_t(\omega) = \sum_{\ell,m}^{N_z} (-1)^{\ell+m} e^{i\omega t_{\ell m}^{(0)}}\, t_{\ell m}^{(0)}\,, \tag{S8}$$

$$I_t'(\omega,\varphi) = -\frac{2}{\omega_0}\sum_{\ell,m}^{N_z} (-1)^{\ell+m} e^{i\omega t_{\ell m}^{(0)}}\, t_{\ell m}^{(0)}\,\mathfrak{f}'(T_{\ell m}^{(0)})\,. \tag{S9}$$

For the situation of an equidistant spacing, the double sum can be reorganized as a sum over pairs. The first summation is over pairs with the same distance, $s = \ell - m$, while the second sum is over the different values $M = (m + \ell)/2$ that these pairs will have

$$I_t(\omega) = \sum_{s=-N_z+1}^{N_z-1} e^{i\omega \mathfrak{t}_s^{(0)}}\, \mathfrak{t}_s^{(0)} \sum_{M=1+|s|/2}^{N_z-|s|/2} (-1)^{2M} \tag{S10}$$

$$I_t'(\omega,\varphi) = -\frac{2}{\omega_0}\sum_{s=-N_z+1}^{N_z-1} e^{i\omega \mathfrak{t}_s^{(0)}}\, \mathfrak{t}_s^{(0)} \sum_{M=1+|s|/2}^{N_z-|s|/2} (-1)^{2M}\,\mathfrak{f}'(t_M^{(0)}(\varphi)) \tag{S11}$$

where we abbreviated $\mathfrak{t}_s^{(0)} := t_s^{(0)}(\varphi{=}0) = \pi s/\omega_0$. Using the relation

$$\sum_{M=1+|s|/2}^{N_z-|s|/2} (-1)^{2M} = (-1)^s(N_z - |s|) \tag{S12}$$

we can simplify

$$I_t(\omega) = \frac{\pi}{\omega_0} \sum_{s=-N_z+1}^{N_z-1} e^{i\pi(\omega/\omega_0+1)s}\, s\,(N_z - |s|) \tag{S13}$$

$$I_t'(\omega,\varphi) = \frac{-2\pi}{\omega_0^2} \sum_{s=-N_z+1}^{N_z-1} e^{i\pi(\omega/\omega_0+1)s}\, s\,(N_z - |s|)\, \bar{\mathfrak{f}}'(s;\varphi)\,; \tag{S14}$$

in the last line we have introduced an average chirp

$$\bar{\mathfrak{f}}'(s;\varphi) := \frac{1}{(N_z - |s|)} \sum_{M=1+|s|/2}^{N_z-|s|/2} \mathfrak{f}'(t_M^{(0)}(\varphi)) \tag{S15}$$

motivated by the observation that a factor $(-1)^{2M-|s|}$ in the M-summation can be replaced by unity. In the special situation where $\bar{\mathfrak{f}}'(s,\varphi)$ is independent of s and φ, we have $I_t'/I_t = -2\bar{\mathfrak{f}}'/\omega_0$; with Eq. (17), we obtain

$$\frac{d\omega}{d\varphi} = -2\frac{\omega}{\omega_0}\bar{\mathfrak{f}}'\,. \tag{S16}$$

In the special situation where $\mathfrak{f}(t)$ is linear in t, we recover (17).

In particular, when choosing a sinusoidal pulse (4), the zeros of $\mathbf{k}(t)$ for $\mathbf{k}_0 = 0$ are obtained as

$$t_m = \frac{1}{\omega_0}\left((m+\frac{1}{2})\,\pi - \varphi\right)\left(1 - \frac{f_{\mathrm{chirp}}}{\omega_0}\left((m+\frac{1}{2})\,\pi - \varphi\right)\right), \tag{S17}$$

in the limit of small chirp ($|f_{\mathrm{chirp}}| \ll \omega_0$) and for small $|m|, m \in \mathbb{Z}$ as it is applicable in case of a few-cycle pulse $E(t)$. When comparing to Eq. (S5), we obtain $\bar{\mathfrak{f}}' = f_{\mathrm{chirp}}$.

S4. EVALUATING THE TIME-LOCAL CHIRP OF THE EXPERIMENTAL ELECTRIC FIELD PULSE

In the main text, we have found that $f_{\mathrm{chirp}} = -1.5\,\mathrm{THz}$ is a good choice in Eq. (17) for reproducing experimental CEP shifts, see Fig. 4. In this section, we discuss how well this choice for f_{chirp} matches with the actual shape of the experimental electric field.

The experimental electric field pulse[9] is sketched in Fig. S2 (a) for $\varphi = 0$ and $\varphi = \pi/2$. We evaluate the "time-local chirp" $\mathfrak{f}'(t_M^{(0)}(\varphi))$ which is the key quantity in our analysis for general pulses in Appendix S3. $\mathfrak{f}'(t_M^{(0)}(\varphi))$ follows from Eq. (S5), $\mathfrak{f}'(t_M^{(0)}(\varphi)) = 1 - t_m(\varphi)/t_m^{(0)}(\varphi)$, where $t_m^{(0)}$, t_m are determined from the experimental pulse $\varphi = \pi/2$. The result is sketched in Fig. S2. We observe that close to $M = 0$, we have a constant local chirp $\mathfrak{f}' \approx -0.92\,\mathrm{THz}$ (giving $-2\pi\bar{\mathfrak{f}}'/\omega_0 \approx 0.037$ with $\omega_0 = 2\pi \cdot 25\,\mathrm{THz}$) while for roots $|M| > 1$, the local chirp is not constant. Thus, higher-order derivatives of $\mathfrak{f}$ become important that are not included in the analysis in Appendix S3 and in our analytical result (17).

Please note, that, compared to the data in Ref. 9, we have redefined the CEP, $-\varphi \to \varphi + 2\pi$, to match the definition in Ref. 9 to the definition in our work.

S5. PARAMETERS OF THE FITS REPORTED IN FIG. 4

In Table S1, we report the full set of fit parameters obtained from the fitting in Fig. 4.

S6. CEP-DEPENDENT EMISSION INTENSITY FOR MODIFIED CHIRP

When employing SBE simulations, we can easily modify f_{chirp} in Eq. (4). To test the prediction $d\omega/d\varphi \propto f_{\mathrm{chirp}}$ from Eq. (17), we double the chirp from $f_{\mathrm{chirp}} = -1.25\,\mathrm{THz}$ (Fig. 2) to $f_{\mathrm{chirp}} = -2.5\,\mathrm{THz}$ [Fig. S3 (a)] and we observe a stronger tilt of the extremal lines of $I(\omega)$ in the (ω,φ)-plane. When changing the sign of the chirp from $f_{\mathrm{chirp}} = -1.25\,\mathrm{THz}$ (Fig. 2) to $f_{\mathrm{chirp}} = 1.25\,\mathrm{THz}$ [Fig. S3 (b)], the direction of the tilt is reversed, in agreement with the sign change of $d\omega/d\varphi$ present in Eq. (17).

TABLE S1: Fit parameters α, β, γ of the fits $\omega(\varphi) = \omega_0[\alpha + \beta(\varphi - \bar{\varphi}) + \gamma(\varphi - \bar{\varphi})^2]$ reported in Fig. 4, as function of the average frequency $\bar{\omega}$ of the line segment. We also report the average CEP $\bar{\varphi}$ of the line segments.

$\bar{\omega}/\omega_0$	13.4	13.5	13.6	14.8	15.3	15.8	17.0	17.5	18.1	20.1
α	−0.02	0.01	0.00	−0.01	−0.01	−0.01	−0.03	−0.04	0.00	−0.01
$2\pi\beta$	1.81	2.00	1.89	1.86	2.23	2.25	2.19	2.24	2.39	2.84
γ	0.02	−0.02	0.01	0.02	0.00	0.00	0.00	0.02	−0.01	0.03
$\bar{\varphi}/\pi$	1.1	2.1	0.3	2.2	1.6	1.2	1.3	0.9	0.4	1.3

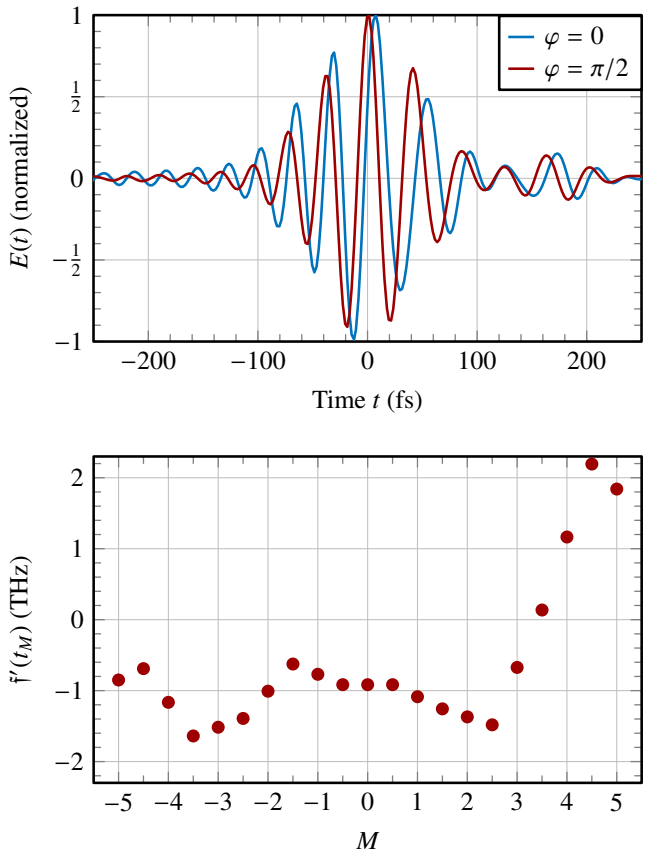

FIG. S2: Top: Experimental pulse shapes from Ref. 9. Bottom: Chirp-like shifting $\mathfrak{f}'(t_M^{(0)}(\varphi{=}\pi/2))$ evaluated from Eq. (S5) for the experimental pulse shape.

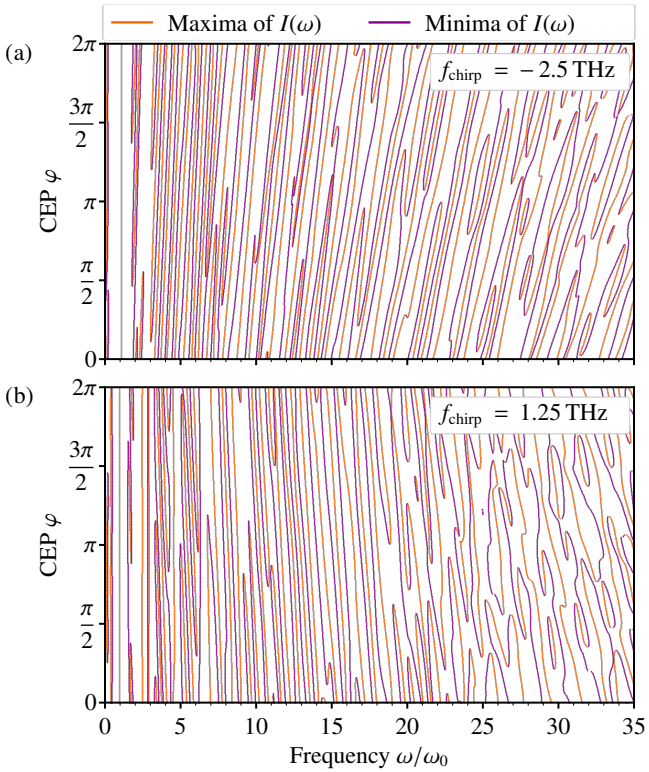

FIG. S3: Local extrema of $I(\omega)$ as in Fig. 2 (b), but with a different chirp of the driving field (4), (a) $f_{\text{chirp}} = -2.5$ THz and (b) $f_{\text{chirp}} = 1.25$ THz.